Topographic divergence of atypical cortical asymmetry and atrophy patterns in temporal lobe epilepsy

Bo-yong Park,[1,2,3] Sara Larivière,[1] Raul Rodríguez-Cruces,[1] Jessica Royer,[1] Shahin Tavakol,[1] Yezhou Wang,[1] Lorenzo Caciagli,[4,5,6] Maria Eugenia Caligiuri,[7] Antonio Gambardella,[7,8] Luis Concha,[9] Simon S. Keller,[10,11] Fernando Cendes,[12] Marina K. M. Alvim,[12] Clarissa Yasuda,[12] Leonardo Bonilha,[13] Ezequiel Gleichgerrcht,[14] Niels K. Focke,[15] Barbara A. K. Kreilkamp,[15] Martin Domin,[16] Felix von Podewils,[17] Soenke Langner,[18] Christian Rummel,[19] Michael Rebsamen,[19] Roland Wiest,[19] Pascal Martin,[20] Raviteja Kotikalapudi,[20,21] Benjamin Bender,[21] Terence J. O'Brien,[22,23] Meng Law,[22] Benjamin Sinclair,[22,23] Lucy Vivash,[22,23] Patrick Kwan,[22,23] Patricia M. Desmond,[24] Charles B. Malpas,[23] Elaine Lui,[24] Saud Alhusaini,[25,26] Colin P. Doherty,[27,28] Gianpiero L. Cavalleri,[25,28] Norman Delanty,[25,28] Reetta Kälviäinen,[29,30] Graeme D. Jackson,[31] Magdalena Kowalczyk,[31] Mario Mascalchi,[32] Mira Semmelroch,[31] Rhys H. Thomas,[33] Hamid Soltanian-Zadeh,[34,35] Esmaeil Davoodi-Bojd,[36] Junsong Zhang,[37] Matteo Lenge,[38,39] Renzo Guerrini,[38] Emanuele Bartolini,[40] Khalid Hamandi,[41,42] Sonya Foley,[41] Bernd Weber,[43] Chantal Depondt,[44] Julie Absil,[45] Sarah J. A. Carr,[46] Eugenio Abela,[46] Mark P. Richardson,[46] Orrin Devinsky,[47] Mariasavina Severino,[48,49] Pasquale Striano,[48,49] Costanza Parodi,[48,49] Domenico Tortora,[48,49] Sean N. Hatton,[50] Sjoerd B. Vos,[4,5,51] John S. Duncan,[4,5] Marian Galovic,[4,5,52] Christopher D. Whelan,[53] Núria Bargalló,[54,55] Jose Pariente,[54] Estefania Conde-Blanco,[56] Anna Elisabetta Vaudano,[57,58] Manuela Tondelli,[57,58] Stefano Meletti,[57,58] Xiang-Zhen Kong,[59,60] Clyde Francks,[59,61] Simon E. Fisher,[59,61] Benoit Caldairou,[62] Mina Ryten,[63,64,65] Angelo Labate,[66] Sanjay M. Sisodiya,[4,5] Paul M. Thompson,[67] Carrie R. McDonald,[68] Andrea Bernasconi,[62] Neda Bernasconi[62] and Boris C. Bernhardt[1]

Temporal lobe epilepsy, a common drug-resistant epilepsy in adults, is primarily a limbic network disorder associated with predominant unilateral hippocampal pathology. Structural MRI has provided an *in vivo* window into whole-brain grey matter structural alterations in temporal lobe epilepsy relative to controls, by either mapping (i) atypical inter-hemispheric asymmetry; or (ii) regional atrophy. However, similarities and differences of both atypical asymmetry and regional atrophy measures have not been systematically investigated.

Here, we addressed this gap using the multisite ENIGMA-Epilepsy dataset comprising MRI brain morphological measures in 732 temporal lobe epilepsy patients and 1418 healthy controls. We compared spatial distributions of grey matter asymmetry and atrophy in temporal lobe epilepsy, contextualized their topographies relative to spatial

gradients in cortical microstructure and functional connectivity calculated using 207 healthy controls obtained from Human Connectome Project and an independent dataset containing 23 temporal lobe epilepsy patients and 53 healthy controls and examined clinical associations using machine learning.

We identified a marked divergence in the spatial distribution of atypical inter-hemispheric asymmetry and regional atrophy mapping. The former revealed a temporo-limbic disease signature while the latter showed diffuse and bilateral patterns. Our findings were robust across individual sites and patients. Cortical atrophy was significantly correlated with disease duration and age at seizure onset, while degrees of asymmetry did not show a significant relationship to these clinical variables.

Our findings highlight that the mapping of atypical inter-hemispheric asymmetry and regional atrophy tap into two complementary aspects of temporal lobe epilepsy-related pathology, with the former revealing primary substrates in ipsilateral limbic circuits and the latter capturing bilateral disease effects. These findings refine our notion of the neuropathology of temporal lobe epilepsy and may inform future discovery and validation of complementary MRI biomarkers in temporal lobe epilepsy.

1   Multimodal Imaging and Connectome Analysis Laboratory, McConnell Brain Imaging Centre, Montreal Neurological Institute and Hospital, McGill University, Montreal, QC, Canada
2   Department of Data Science, Inha University, Incheon, Republic of Korea
3   Center for Neuroscience Imaging Research, Institute for Basic Science, Suwon, Republic of Korea
4   Department of Clinical and Experimental Epilepsy, UCL Queen Square Institute of Neurology, London, UK
5   MRI Unit, Epilepsy Society, Chalfont St Peter, Buckinghamshire, UK
6   Department of Bioengineering, University of Pennsylvania, Philadelphia, PA, USA
7   Neuroscience Research Center, University Magna Græcia, Catanzaro, CZ, Italy
8   Institute of Neurology, University Magna Græcia, Catanzaro, CZ, Italy
9   Institute of Neurobiology, Universidad Nacional Autónoma de México, Querétaro, México
10 Institute of Systems, Molecular and Integrative Biology, University of Liverpool, Liverpool, UK
11 Walton Centre NHS Foundation Trust, Liverpool, UK
12 Department of Neurology, University of Campinas–UNICAMP, Campinas, São Paulo, Brazil
13 Department of Neurology, Emory University, Atlanta, GA, USA
14 Department of Neurology, Medical University of South Carolina, Charleston, SC, USA
15 Department of Neurology, University Medical Center Göttingen, Göttingen, Germany
16 Institute of Diagnostic Radiology and Neuroradiology, Functional Imaging Unit, University Medicine Greifswald, Greifswald, Germany
17 Department of Neurology, University Medicine Greifswald, Greifswald, Germany
18 Institute of Diagnostic Radiology and Neuroradiology, University Medicine Greifswald, Greifswald, Germany
19 Support Center for Advanced Neuroimaging (SCAN), University Institute of Diagnostic and Interventional Neuroradiology, University Hospital Bern, Bern, Switzerland
20 Department of Neurology and Epileptology, Hertie Institute for Clinical Brain Research, University of Tübingen, Tübingen, Germany
21 Department of Radiology, Diagnostic and Interventional Neuroradiology, University Hospital Tübingen, Tübingen, Germany
22 Department of Neuroscience, Central Clinical School, Alfred Hospital, Monash University, Melbourne, Victoria, Australia
23 Departments of Medicine, The Royal Melbourne Hospital, The University of Melbourne, Parkville, Victoria, Australia
24 Department of Radiology, The Royal Melbourne Hospital, The University of Melbourne, Parkville, Victoria, Australia
25 Department of Molecular and Cellular Therapeutics, The Royal College of Surgeons in Ireland, Dublin, Ireland
26 Department of Neurology, Yale University School of Medicine, New Haven, CT, USA
27 Department of Neurology, St James' Hospital, Dublin, Ireland
28 FutureNeuro SFI Research Centre, Dublin, Ireland
29 Epilepsy Center, Neuro Center, Kuopio University Hospital, Member of the European Reference Network for Rare and Complex Epilepsies EpiCARE, Kuopio, Finland
30 Faculty of Health Sciences, School of Medicine, Institute of Clinical Medicine, University of Eastern Finland, Kuopio, Finland
31 Florey Institute of Neuroscience and Mental Health, University of Melbourne, Melbourne, Victoria, 3010, Australia
32 Neuroradiology Research Program, Meyer Children Hospital of Florence, University of Florence, Florence, Italy
33 Transitional and Clinical Research Institute, Newcastle University, Newcastle upon Tyne, UK
34 Control and Intelligent Processing Center of Excellence (CIPCE), School of Electrical and Computer Engineering, University of Tehran, Tehran, Iran
35 Departments of Research Administration and Radiology, Henry Ford Health System, Detroit, MI, USA

36 Department of Neurology, Henry Ford Health System, Detroit, MI, USA
37 Department of Artificial Intelligence, Xiamen University, Xiamen, China
38 Child Neurology Unit and Laboratories, Neuroscience Department, Children's Hospital A. Meyer-University of Florence, Florence, Italy
39 Functional and Epilepsy Neurosurgery Unit, Neurosurgery Department, Children's Hospital A. Meyer-University of Florence, Florence, Italy
40 USL Centro Toscana, Neurology Unit, Nuovo Ospedale Santo Stefano, Prato, Italy
41 Cardiff University Brain Research Imaging Centre (CUBRIC), College of Biomedical Sciences, Cardiff University, Cardiff, UK
42 The Welsh Epilepsy Unit, Department of Neurology, University Hospital of Wales, Cardiff, UK
43 Institute of Experimental Epileptology and Cognition Research, University Hospital Bonn, Bonn, Germany
44 Department of Neurology, Hôpital Erasme, Université Libre de Bruxelles, Brussels, Belgium
45 Department of Radiology, Hôpital Erasme, Université Libre de Bruxelles, Brussels, Belgium
46 Division of Neuroscience, Institute of Psychiatry, Psychology and Neuroscience, King's College London, UK
47 Department of Neurology, NYU Grossman School of Medicine, New York, NY, USA
48 IRCCS Istituto Giannina Gaslini, Genova, Italy
49 Department of Neurosciences, Rehabilitation, Ophthalmology, Genetics, Maternal and Child Health, University of Genova, Genova, Italy
50 Department of Neurosciences, Center for Multimodal Imaging and Genetics, University of California San Diego, La Jolla, CA, USA
51 Centre for Medical Image Computing, University College London, London, UK
52 Department of Neurology, Clinical Neuroscience Center, University Hospital and University of Zurich, Zurich, Switzerland
53 Department of Molecular and Cellular Therapeutics, The Royal College of Surgeons in Ireland, Dublin, Ireland
54 Magnetic Resonance Image Core Facility, Institut d'Investigacions Biomèdiques August Pi i Sunyer (IDIBAPS), Barcelona, Spain
55 Department of Radiology CDIC, Hospital Clinic Barcelona, Barcelona, Spain
56 Epilepsy Unit, Department of Neurology, Hospital Clínic, Barcelona, Spain
57 Neurology Unit, Azienda Ospedaliero-Universitaria of Modena, OCB Hospital, Modena, Italy
58 Department of Biomedical, Metabolic, and Neural Sciences, Center for Neuroscience and Neurotechnology, University of Modena and Reggio Emilia, Modena, Italy
59 Language and Genetics Department, Max Planck Institute for Psycholinguistics, Nijmegen, The Netherlands
60 Department of Psychology and Behavioral Sciences, Zhejiang University, Hangzhou, China
61 Donders Institute for Brain, Cognition and Behaviour, Radboud University, Nijmegen, The Netherlands
62 Neuroimaging of Epilepsy Laboratory, McConnell Brain Imaging Centre, Montreal Neurological Institute and Hospital, McGill University, Montreal, QC, Canada
63 Department of Neurodegenerative Disease, Queen Square Institute of Neurology, University College London, London, UK
64 NIHR Great Ormond Street Hospital Biomedical Research Centre, University College London, London, UK
65 Department of Genetics and Genomic Medicine, Great Ormond Street Institute of Child Health, University College London, London, UK
66 Neurology, BIOMORF Department, University of Messina, Messina, Italy
67 Imaging Genetics Center, Mark & Mary Stevens Institute for Neuroimaging and Informatics, USC Keck School of Medicine, Los Angeles, CA, USA
68 Department of Psychiatry, Center for Multimodal Imaging and Genetics, University of California San Diego, La Jolla, CA, USA

Correspondence to: Bo-yong Park
Department of Data Science, Inha University, Incheon, Republic of Korea
E-mail: boyong.park@inha.ac.kr

Correspondence may also be addressed to: Boris C. Bernhardt, PhD
Multimodal Imaging and Connectome Analysis Lab, McConnell Brain Imaging Centre
Montreal Neurological Institute and Hospital, McGill University, Montreal, Quebec, Canada
E-mail: boris.bernhardt@mcgill.ca

Introduction

Temporal lobe epilepsy (TLE) is the most common drug-resistant epilepsy in adults. Its hallmark is pathology of mesiotemporal structures, notably the hippocampus, entorhinal cortex, amygdala and temporal pole.[1–5] The degree of atrophy in these regions correlates with the tendency to express epileptic activity.[6,7] Moreover, unilateral anteromesial resection leads to worthwhile improvement in approximately 90% of patients and long-term seizure freedom in more than 50%.[8–10]

MRI can identify the pathological substrate of TLE *in vivo* and lateralize and define the surgical target. Indeed, MRI has provided biomarker candidates for TLE diagnostics, prognostics and disease staging.[11–13] MRI analyses in TLE traditionally focus on manually or automatically delineating individual mesiotemporal structures, followed by (i) the analysis of inter-hemispheric grey matter asymmetry; or (ii) the regional comparison of morphometric measures in patients relative to healthy controls. Studies focusing on mesiotemporal grey matter consistently reported atrophy and marked asymmetry, reaffirming that TLE is primarily a limbic disorder.[10,14–21]

With advancements and automation of image processing techniques, quantitative MRI analysis has been extended to the whole-brain level using volumetric analysis and voxel-based morphometry [20,22–27] as well as surface-based cortical thickness analysis.[28–32] These studies have mainly been cross-sectional regional comparisons between TLE and healthy controls, and explored patterns of inter-hemispheric asymmetry in TLE only sporadically. Whole-brain analyses often showed asymmetric mesiotemporal damage, and also revealed widespread and bilateral decreases in cortical grey matter outside the mesiotemporal lobe, with neither a limbic nor lateralized predominance.[31–35] Similar findings were confirmed by a multisite initiative aggregating and analysing brain morphometric measures in common epilepsies.[34,36]

Outside the mesiotemporal regions, the scarcity of asymmetry analyses precludes insights into how similar or different patterns of atypical structural asymmetry are relative to patterns of regional atrophy in TLE. Analysing both atrophy and asymmetry features could inform the development of individualized MRI biomarkers.[19,20,37,38] Moreover, comparing these patterns could clarify whether these reflect different disease processes. One emerging family of approaches stratifies cortical areas along spatial gradients of cortical microstructure and connectivity.[39–41] Cortical areas indeed show variable microstructural characteristics, often following sensory–fugal spatial gradients that relate to plasticity and neural excitability.[35,41–46] For example, paralimbic circuits differ from sensory networks by having an agranular architecture with only subtle laminar differentiation and relatively low myelin content, while sensorimotor areas have a marked layer IV and higher intracortical myelin.[35,47–50] Complementing these microstructural variations, recent work has shown gradients of functional connectivity running from sensorimotor networks towards heteromodal systems, notably the default mode network.[39] Contextualizing atrophy and atypical asymmetry patterns along these microstructural and functional connectivity gradients may shed light on potential anatomical determinants of cortical pathology in TLE.

We used the ENIGMA-Epilepsy dataset to map the topography of atypical inter-hemispheric asymmetry and regional atrophy in 732 individuals with TLE and 1418 healthy controls. Using a multisite mega-analysis, we systematically assessed the commonalities and divergences of these spatial patterns. We further contextualized findings with respect to microstructural and functional connectivity gradients, derived from parallel myelin-sensitive microstructural MRI and resting-state functional acquisitions,[39,41,51] obtained from both Human Connectome Project (HCP; 207 healthy controls) as well as a local cohort of TLE patients and controls (23 TLE and 53 healthy controls). We formulated the following hypotheses: (i) the spatial distribution of TLE-related cortical asymmetry and atrophy would differ, with the former being particularly temporo-limbic; and (ii) atypical asymmetry and atrophy maps would relate to cortical gradients, with the asymmetry map being more closely related to the primary temporo-limbic gradients derived from cortical microstructure. We also assessed whether inter-hemispheric asymmetry and regional atrophy mapping would show differential associations with clinical parameters, notably effects of disease duration and age of onset. In addition to benefiting from the high power of ENIGMA-Epilepsy, we validated the consistency of our findings at the level of single patients and individual sites.

Materials and methods

Participants

We analysed 2150 T_1-weighted MRI datasets from 732 patients with TLE and confirmed/suspected mesiotemporal sclerosis (55% females, mean age $\pm$ SD = 38.56 $\pm$ 10.61 years; 391/341 left/right TLE) and 1418 healthy controls (55% females, mean age $\pm$ SD = 33.76 $\pm$ 10.54 years) obtained from 19 different sites via the Epilepsy Working Group of ENIGMA[34,36,52] (Table 1). Individuals with epilepsy were diagnosed by epilepsy specialists at each centre according to classifications of the International League Against Epilepsy.[53] TLE patients were diagnosed based on electroclinical and neuroimaging findings. Participants with a primary progressive disease (e.g. Rasmussen's encephalitis), visible malformations of cortical development, or prior neurosurgery were excluded. For each site, local institutional review boards and ethics committees approved each included cohort study and written informed consent was provided according to local requirements.

Gradients were derived from two independent cohorts containing healthy controls and patients with TLE: (i) A sample of 207 unrelated healthy young adults (60% females, mean age $\pm$ SD = 28.73 $\pm$ 3.73 years) from the HCP[54]; and (ii) a sample of 53 healthy controls (38% females, mean age $\pm$ SD = 30.84 $\pm$ 7.59 years) and 23 TLE patients (52% females, mean age $\pm$ SD = 37.29 $\pm$ 11.96 years) from our local site at the MNI (microstructure-informed connectomics; MICs). All participants gave written and informed consent.

Data preprocessing

ENIGMA data

Participants underwent T_1-weighted scans at each of the 19 centres, with acquisition protocols detailed elsewhere.[34] Imaging data were processed by each centre through the standard ENIGMA workflow described in Supplementary material and Supplementary Fig. 1.

HCP data

T_1- and T_2-weighted, as well as resting-state functional MRI (rs-fMRI) data, were obtained using a Siemens Skyra 3 T at Washington University.[54] The T_1-weighted images were acquired using a magnetization-prepared rapid gradient echo sequence [repetition time (TR) = 2400 ms; echo time (TE) = 2.14 ms; inversion time (TI) = 1000 ms; flip angle = 8°; field of view (FOV) = 224 × 224 mm^2; voxel size = 0.7 mm isotropic; and number of slices = 256]. T_2-weighted data were obtained with a T_2-SPACE sequence (TR = 3200 ms; TE = 565 ms; flip angle = variable; FOV = 224 × 224 mm^2; voxel size = 0.7 mm isotropic; and number of slices = 256).

Table 1 Demographic information of individuals with TLE and site-matched controls

Information	ENIGMA-Epilepsy		HCP (HC)	MICs	
	TLE	HC		TLE	HC
n	732	1418	207	23	53
Age, years	38.56 ± 10.61	33.76 ± 10.54	28.73 ± 3.73	37.29 ± 11.96	30.84 ± 7.59
Sex, male: female	329:403	643:775	83:124	11:12	33:20
Age at onset, years	16.07 ± 12.27	N/A	N/A	21.59 ± 11.65	N/A
Side of focus, left/right	391/341	N/A	N/A	15/7 (1 bilateral)	N/A
Duration of illness, years	22.74 ± 14.06[a]	N/A	N/A	15.82 ± 12.45	N/A

Means and SDs are reported. HC = healthy control; N/A = not available.
[a]Information available in 695 TLE patients.

The rs-fMRI data were collected using a gradient-echo echo-planar imaging sequence (TR = 720 ms; TE = 33.1 ms; flip angle = 52°; FOV = 208 × 180 mm^2; voxel size = 2 mm isotropic; number of slices = 72; and number of volumes = 1200 per time series). During the rs-fMRI scan, participants were instructed to keep their eyes open, looking at a fixation cross. Two sessions of rs-fMRI data were acquired; each contained data of left-to-right and right-to-left phase-encoded directions, providing up to four time series per participant. HCP data underwent minimal preprocessing pipelines using FSL, FreeSurfer and Workbench,[55–57] briefly summarized in Supplementary material and Supplementary Fig. 1.

MICs data

Data were acquired on a Siemens Prisma 3T scanner. Acquisition parameters were similar to the HCP dataset (T$_1$-weighted: TR = 2300 ms; TE = 3.14 ms; TI = 900 ms; flip angle = 9°; FOV = 256 × 180 mm^2; voxel size = 0.8 mm isotropic; and number of slices = 320; quantitative T$_1$: same as T$_1$-weighted except for TR = 5000 ms and TE = 2.9 ms; TI = 940 ms; flip angle 1 = 4°; flip angle 2 = 5°; rs-fMRI: TR = 600 ms; TE = 30 ms; flip angle = 52°; FOV = 240 × 240 mm^2; voxel size = 3 mm isotropic; number of slices = 48; and number of volumes = 700). MICs data were preprocessed using micapipe (https://github.com/MICA-MNI/micapipe; last accessed February 5, 2022), which integrates AFNI, FSL, FreeSurfer, ANTs and Workbench.[55–59] Details are described in Supplementary material and Supplementary Fig. 1.

Atypical inter-hemispheric cortical asymmetry and regional atrophy

We calculated inter-hemispheric asymmetry of cortical thickness using the following formula: $AI = (ipsi − contra) / |(ipsi + contra)/2|$,[19,60,61] where AI is asymmetry index and $ipsi$ and $contra$ are the cortical thickness of ipsilateral and contralateral areas, respectively. The asymmetry index was z-normalized relative to site-matched pooled controls and sorted into ipsilateral/contralateral to the focus.[62] It was then harmonized across different sites by adjusting for age, sex and intracranial volume using ComBat, a batch-effect correction tool that uses a Bayesian framework to improve the stability of the parameter estimates.[63,64] We compared the harmonized asymmetry index between individuals with TLE and controls using a general linear model implemented in SurfStat.[65] Multiple comparisons across brain regions were corrected using the FDR procedure.[66] In addition to parcel-wise analysis, we stratified asymmetry measures according to seven intrinsic functional communities (visual, somatomotor, dorsal attention, ventral attention, limbic, frontoparietal and default mode)[67] and lobes (frontal, parietal, temporal, occipital, cingulate

and insular cortex). In addition to the atypical asymmetry index, we assessed cortical atrophy in TLE patients relative to controls. Cortical thickness measures were z-normalized, flipped hemispheres of right TLE and harmonized as for the asymmetry index. We compared the harmonized cortical thickness between the groups and the findings were multiple-comparison corrected using FDR[66] as well as stratified according to functional communities and lobes.

Association to gradients of cortical microstructure and function

We assessed topographic underpinnings of TLE-related asymmetry and atrophy through spatial correlation analysis with microstructural and functional gradients, the principal eigenvectors explaining spatial shifts in microstructural similarity and functional connectivity.[39,41] Gradients were defined using two alternative datasets, either based on both the HCP (i.e. healthy controls) or based on the MICs (i.e. healthy controls and TLE patients), using BrainSpace (https://github.com/MICA-MNI/BrainSpace; last accessed 5 February 2022).[51] Specifically, we calculated a parcel-to-parcel affinity matrix for each feature using a normalized angle kernel considering the top 10% entries for each parcel. As in prior work,[39,45,51,68–74] we opted for diffusion map embedding,[75] a non-linear technique that is robust to noise and computationally efficient.[76,77] It is controlled by two parameters, α and t, where α controls the influence of the density of sampling points on the manifold ($\alpha = 0$, maximal influence; $\alpha = 1$, no influence) and t scales eigenvalues of the diffusion operator. The parameters were set as $\alpha = 0.5$ and $t = 0$ to retain the global relations between data-points in the embedded space, following prior applications.[39,41,45,51,69,78] We examined associations of the estimated gradients with cortical asymmetry in a single hemisphere and atrophy patterns in both hemispheres via linear correlations, where significance was determined using 1000 non-parametric spin tests that account for spatial autocorrelation[79] implemented in the ENIGMA Toolbox.[80]

Consistency mapping across sites and individuals

We assessed the robustness of our findings within a probabilistic framework at the single site and subject level. The consistency across sites was measured by calculating linear correlations between epilepsy-related asymmetry and atrophy findings and gradients for each site. For individual-level consistency, we counted how many participants are comprised within a specific threshold (i.e. $z < −2$). The counts were divided by the number of participants to obtain a probability map. Thus, the consistency probability indicates that the top N% patients showed extreme asymmetry or cortical atrophy measures in a given region. The consistency

probability was correlated with microstructural and functional gradients, with 1000 non-parametric spin tests.[79,80]

Associations with clinical variables

We associated clinical variables of duration and onset of epilepsy with atypical asymmetry index and cortical atrophy using supervised machine learning. We utilized 5-fold nested cross-validation[76,81–83] with least absolute shrinkage and selection operator (LASSO) regression.[84] We split the dataset into training (4/5) and test (1/5) partitions, and each training partition was further split into inner training and testing folds using another 5-fold cross-validation. Within the inner fold, LASSO finds a set of non-redundant features (i.e. atypical asymmetry index or cortical atrophy of brain regions) that could explain the dependent variable (i.e. disease duration or onset age). Using a linear regression, we predicted the clinical variables of inner fold test data using the features of the selected brain regions. The model with best accuracy (i.e. minimum mean absolute error, MAE) across the inner folds was applied to the test partition of the outer fold and the clinical variables of outer fold test data were predicted. We repeated this procedure 100 times with different training and test partitions to avoid subject selection bias. We assessed the prediction accuracy by calculating linear correlations between the actual and predicted clinical variables with their 95% confidence interval across 100 repetitions, as well as MAE. The significance of the correlation between actual and predicted values was assessed using 1000 permutation tests by randomly shuffling participant indices. A null distribution was constructed, and it was deemed significant if the real correlation value did not belong to 95% of the distribution (two-tailed $P < 0.05$). We compared our model with the baseline model [i.e. predicted clinical variable = mean(training set clinical variable)] and improved prediction performance of our model was assessed using Meng's z-test.[85] To assess whether the frequency of the selected brain regions derived from LASSO regression across cross-validations and repetitions is related to microstructural and functional gradients, we calculated spatial correlations between cortex-wide probability distributions and each of the gradients. Significance was assessed using 1000 spin tests.[79,80] As a post-hoc analysis, we correlated the cortical features of the highly probable regions (selected probability > 0.5) and clinical variables, and the significance was calculated based on 1000 permutation tests by randomly shuffling participant indices.

Sensitivity analysis
Left and right TLE

To assess whether left and right TLE show consistent results, we repeated assessing atypical cortical asymmetry and atrophy and correlating the effects with gradients for separate left and right TLE subgroups. We furthermore assessed cortical atrophy in individuals with left and right TLE for each hemisphere. We conducted paired *t*-tests to compare cortical atrophy between hemispheres within left or right TLE, and two-sample *t*-tests between left and right TLE. Multiple comparisons were corrected using FDR.[66]

Different density of connectivity matrix

In our main analysis, we estimated microstructural and functional gradients using connectivity matrices with 10% density. We repeated generating the gradients from connectivity matrices with different densities (20%, 30%, 40%, 50%) and correlated with atypical cortical asymmetry and atrophy patterns.

Gradients generated using local dataset

We generated microstructural and functional gradients using a combined dataset of healthy individuals and patients with TLE, to assess consistency of the topographic relationships between TLE-related asymmetry/atrophy and cortical gradients.

Volumetric analysis

We additionally assessed atypical inter-hemispheric asymmetry and regional atrophy patterns of six subcortical regions (amygdala, caudate, nucleus accumbens, pallidum, putamen, thalamus), as well as the hippocampus, defined using the Desikan–Killiany atlas.[86] We estimated the volume of each region, calculated asymmetry index,[19,60,61] z-normalized both asymmetry index and volume of TLE patients relative to controls, flipped hemispheres in right TLE patients and harmonized data across different sites by adjusting for age, sex and intracranial volume using ComBat.[63,64] We compared asymmetry and regional volume between individuals with TLE and controls using a general linear model.[65] Next, we assessed the robustness of atypical asymmetry and atrophy by calculating consistency probability. Lastly, we performed the prediction analysis by considering both cortical thickness and subcortical/hippocampal volume measures using LASSO regression [84] with five fold nested cross-validation.[76,81–83] The prediction procedure was repeated 100 times with different training and test datasets and the performance was measured using linear correlations between the actual and predicted clinical variables with their 95% confidence interval, as well as MAE. We compared our model with the baseline model, and assessed improvement of the prediction performance using Meng's z-test.[85]

Data availability

The data that support the findings of this study are available on request from the corresponding author. The data are not all publicly available in a repository as they contain information that could compromise the privacy of research participants.

Although there are data-sharing restrictions imposed by (i) ethical review boards of the participating sites, and consent documents; (ii) national and trans-national data sharing law, such as General Data Protection Regulation (GDPR); and (iii) institutional processes, some of which require a signed Material Transfer Agreements (MTA) for limited and predefined data use, we welcome sharing data with researchers, requiring only that they submit an analysis plan for a secondary project to the leading team of the Working Group (http://enigma.ini.usc.edu; last accessed 5 February 2022). Once this analysis plan is approved, access to the relevant data will be provided contingent on data availability and local PI approval and compliance with all supervening regulations. If applicable, distribution of analysis protocols to sites will be facilitated.

Results

Atypical inter-hemispheric asymmetry patterns differ from regional cortical atrophy in TLE

We found significant deviations in inter-hemispheric asymmetry in TLE relative to controls, especially in lateral and medial temporal cortex, as well as precuneus, with ipsilateral regions being atypically smaller than contralateral regions ($P_{FDR} < 0.05$; Fig. 1A). Stratifying effects according to intrinsic functional communities,[67] highest deviations in asymmetry were observed in the limbic network followed by default mode and somatomotor networks (Fig. 1B). Lobar analysis identified most marked degrees of atypical
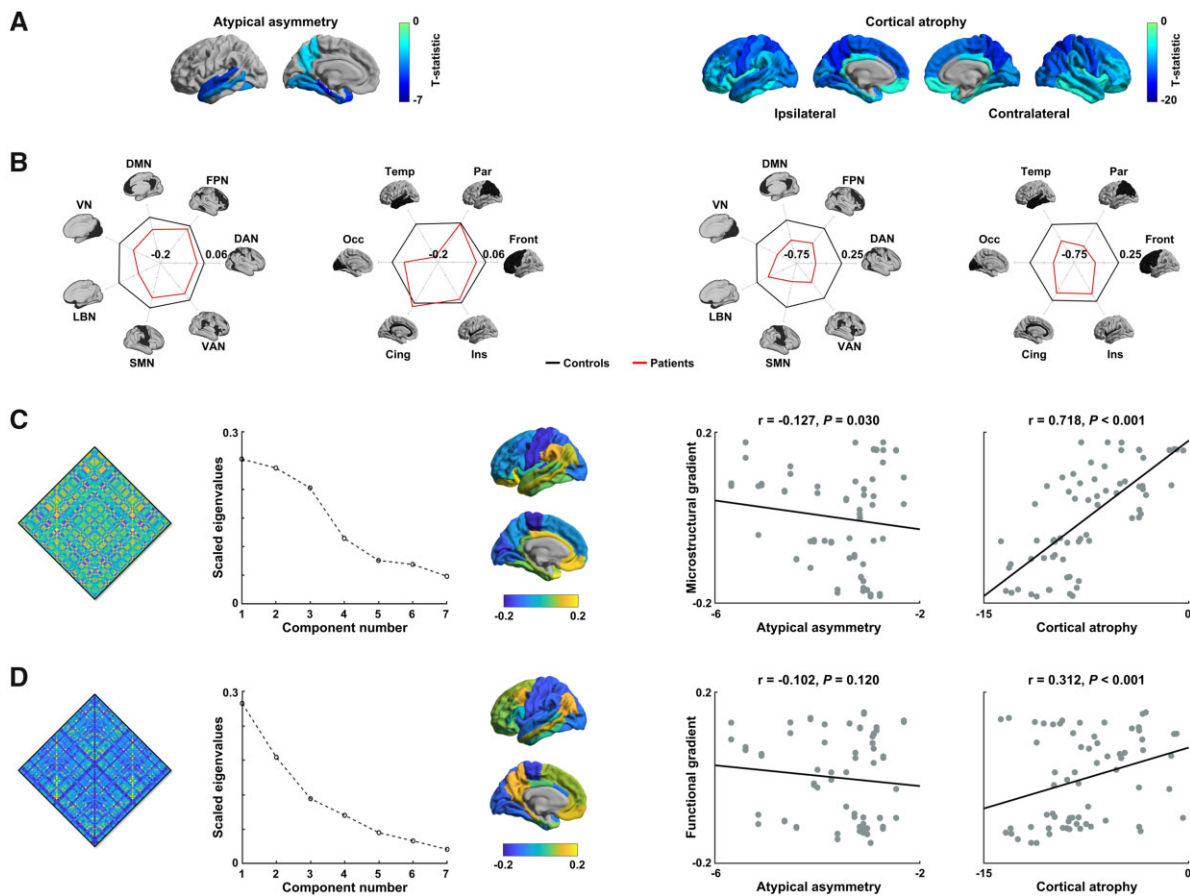
Figure 1 Topography of atypical cortical asymmetry and atrophy patterns in TLE. (**A**) Atypical inter-hemispheric asymmetry of cortical thickness and regional cortical atrophy between individuals with TLE relative to controls, calculated using ENIGMA-Epilepsy dataset. Blue regions indicate significant ipsilateral versus contralateral cortical thickness asymmetry/atrophy in TLE relative to controls. Patient hemispheres are sorted into ipsilateral/contralateral to the seizure focus. (**B**) Effects (i.e. asymmetry index and cortical thickness) are stratified according to seven intrinsic functional communities[67] and major lobes. (**C**) Associations between epilepsy-related findings and microstructural/functional gradients calculated using HCP dataset. Cortex-wide microstructural profile similarity matrix and scree plot describing connectome variance after identification of principal eigenvectors are shown. The first principal eigenvector (microstructural gradient) is shown on the cortical surface. Spatial correlations between the principal microstructural gradient and TLE-related effects (i.e. atypical cortical asymmetry and atrophy) are reported with scatter plots. (**D**) Identical analysis to **C** but based on functional gradients. Cing = cingulate; DAN = dorsal attention network; DMN = default mode network; FPN = frontoparietal control network; Front = frontal; Ins = insular; LBN = limbic network; Occ = occipital; Par = parietal; SMN = somatomotor network; Temp = temporal; VAN = ventral attention network; VN = visual network.

asymmetry in the temporal lobes. Asymmetry patterns of TLE were markedly different from regional differences in bilateral cortical thickness. Indeed, comparing cortical thickness between TLE and healthy controls showed widespread and bilateral cortical thickness reductions in TLE, with strongest effects in precentral, paracentral and superior temporal regions ($P_{FDR} < 0.05$; Fig. 1A). Findings were distributed across somatomotor, dorsal attention and visual networks (Fig. 1B). Similarly, lobar stratification pointed to multilobar effects, most marked in frontal, parietal and occipital lobes in both hemispheres. Notably, spatial correlations between atypical asymmetry and atrophy patterns in a single hemisphere were very low and did not surpass null models with similar autocorrelation ($r = 0.05$, $P = 0.27$).[79]

A diverging topographic landscape of TLE-related atypical asymmetry and atrophy

Next, we assessed spatial associations of epilepsy-related findings with microstructural and functional gradients. The microstructural gradient depicted a continuous differentiation of cortical features between sensory and limbic areas, and was negatively

correlated with atypical asymmetry index ($r = –0.13$, $P_{FDR} = 0.03$), reflecting elevated atypical asymmetry in temporo-limbic cortices in TLE (Fig. 1C). On the other hand, it was positively and markedly correlated with regional atrophy in TLE ($r = 0.72$; $P_{FDR} < 0.001$; Fig. 1C). The difference between these two correlations was significant ($P < 0.001$; Meng's z-test),[85] indicating a dissociation of atypical asymmetry and atrophy patterns with respect to the primary microstructural gradient. The functional gradient differentiated primary sensory from transmodal regions, and did not show a significant association with atypical inter-hemispheric asymmetry in TLE ($r = –0.10$, $P_{FDR} = 0.12$), but a low-to-moderate positive association with regional atrophy ($r = 0.31$, $P_{FDR} < 0.001$; Fig. 1D).

Consistency across sites and individuals

We confirmed the above topographic divergence across individual sites (Fig. 2A) by correlating microstructural and functional gradients with atypical asymmetry and regional atrophy in TLE for each site separately (Fig. 2B). These follow-up analyses confirmed our main findings (Fig. 1C and D) that showed dissociation between atypical asymmetry and atrophy patterns. Multisite analyses were expanded by assessing consistency at the level of
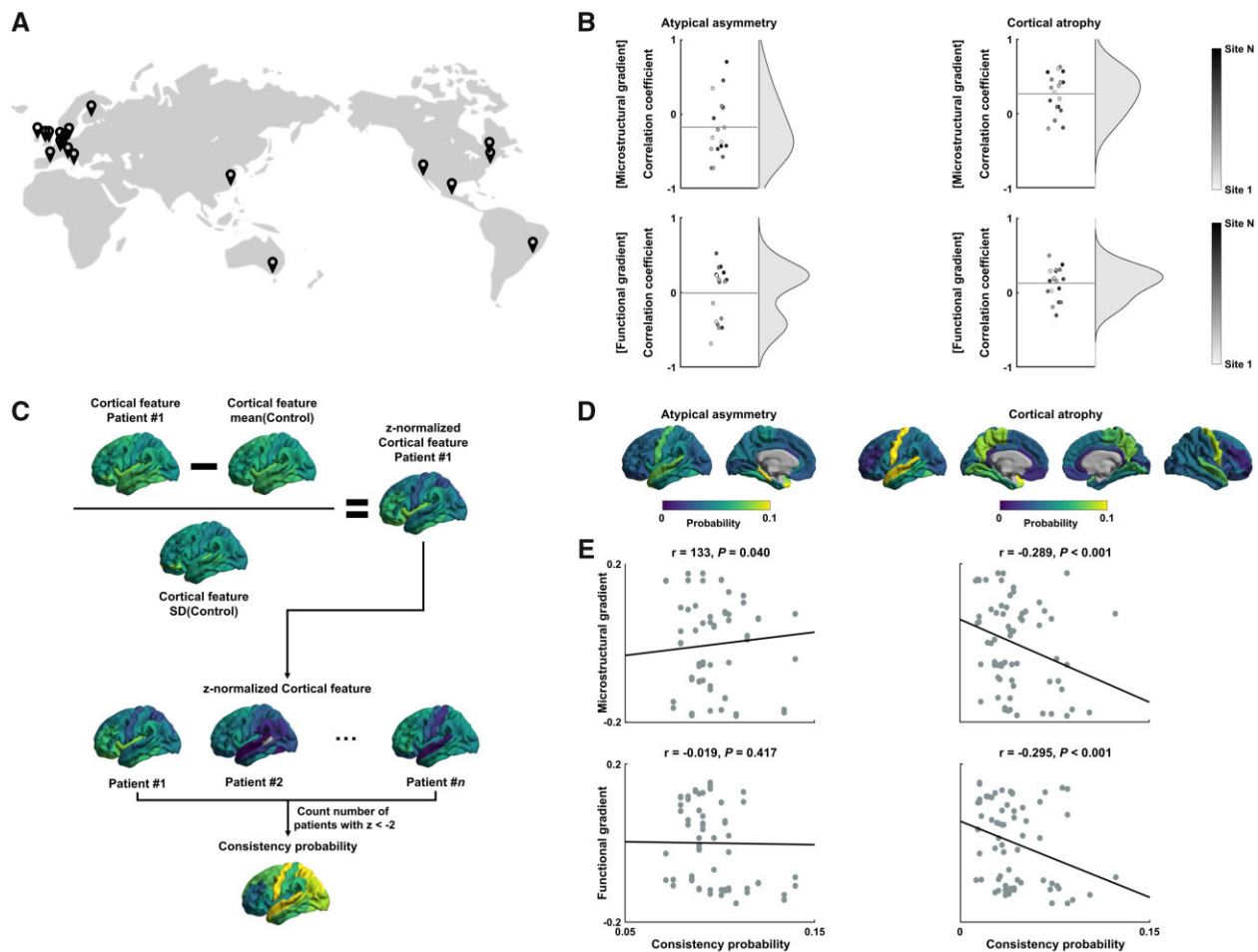
Figure 2 Consistency of atypical cortical asymmetry and atrophy. (**A**) World map of data acquisition sites. (**B**) Spatial correlations between topographic gradients and atypical cortical asymmetry/atrophy patterns of all sites. (**C**) Schema describing the computation of patient-wise consistency probability. The number of patients with large deviations of cortical features (i.e. atypical inter-hemispheric asymmetry or regional cortical atrophy) was counted. (**D**) Consistency probability of atypical cortical asymmetry and atrophy. (**E**) Spatial correlations between consistency probability and topographic gradients.

individual patients (Fig. 2C). Prevalent atypical asymmetry was confirmed in somatomotor and limbic regions (Fig. 2D) and spatial patterns revealed significant associations only with the microstructural gradient ($r = 0.13/–0.02$, $P_{FDR} = 0.04/0.42$ for microstructural/functional gradients; Fig. 2E). The consistency probability of regional cortical atrophy showed higher consistency in sensory, precuneus and temporal regions, and it showed significant negative correlations with both gradients ($r = –0.29/–0.30$, $P_{FDR} < 0.001/ <0.001$), supporting patient-level consistency.

Associations with clinical variables

Utilizing supervised machine learning, we probed associations of both atypical inter-hemispheric asymmetry and regional atrophy with disease duration and age at seizure onset. While cortical atrophy significantly predicted the clinical variables outperforming the baseline model (disease duration: mean $\pm$ SD $r = 0.26 \pm 0.02$, MAE $= 11.38 \pm 0.10$, Meng's z-test $P < 0.001$; age at seizure onset: $r = 0.17 \pm 0.02$, MAE $= 9.91 \pm 0.08$, Meng's z-test $P = 0.01$), atypical asymmetry did not (disease duration: Meng's z-test $P = 0.27$; age at seizure onset: Meng's z-test $P = 0.20$; Fig. 3A,D). Considering cortical atrophy, sensorimotor, medial/lateral temporal, and precuneus were frequently selected across cross-validations as salient features for the prediction for disease duration (Fig. 3A), and

sensorimotor and limbic regions for age at seizure onset (Fig. 3D). As in the main analyses, we observed significant associations of the selected probability with connectome gradients (disease duration: $r = –0.27/–0.34$ $P_{FDR} = 0.002/<0.001$ for microstructural/functional gradients; age at seizure onset: $r = –0.25/0.03$ $P_{FDR} < 0.001/ 0.35$; Fig. 3B and E). Associations in highly probable regions (selected probability > 0.5) were negative, i.e. disease duration/age at seizure onset associated with cortical thickness reductions ($r = –0.30/–0.21$, permutation test $P < 0.001/<0.001$; Fig. 3C and F).

Sensitivity analyses

Several analyses supported robustness of our main findings.

Left and right TLE

We repeated the above analyses in left and right TLE separately. While the degree of asymmetry was stronger in left than right TLE, findings were overall consistent (Supplementary Fig. 2). In the temporal lobe, while both left and right TLE patients showed more pronounced ipsilateral cortical atrophy, ipsilateral atrophy in left TLE was more marked than in right TLE, while contralateral atrophy was stronger in the latter subgroup (Supplementary Fig. 2E and F).

Different density of connectivity matrix

We repeated our analyses by varying the thresholds of microstructural and functional connectivity matrices across different densities (20%, 30%, 40%, 50%). Gradients and their associations with inter-hemispheric asymmetry, as well as regional atrophy, remained consistent (Supplementary Fig. 3).

Gradients generated using local dataset

We also repeated the analysis after building gradients using a different dataset comprising both healthy individuals and patients with TLE. Microstructural and functional gradients were highly similar to those from the HCP dataset, and topographic associations between TLE-related asymmetry/atrophy and cortical gradients remained consistent when using gradients based on a combined dataset of healthy individuals and patients with TLE (Supplementary Fig. 4).

Volumetry of subcortical regions and the hippocampus

We also studied the volume of subcortical structures as well as the hippocampus. While atypical asymmetry and atrophy patterns both supported marked ipsilateral hippocampal effects ($P_{FDR} < 0.05$; Supplementary Fig. 5A), spatial correlations between atypical inter-hemispheric asymmetry and regional atrophy were moderate and not significant ($r = 0.51$, $P = 0.06$). As for the cortical thickness-based results, these findings were consistent across individual subjects (Supplementary Fig. 5B). When we considered both cortical thickness and subcortical/hippocampal volume, we were able to confirm our initial results in that atrophy but not atypical asymmetry related to age at seizure onset, while disease duration was significantly associated with both measures, outperforming the baseline model (atypical asymmetry: $P = 0.004$ for disease duration, $P = 0.14$ for age at seizure onset; atrophy: $P < 0.001$ for both disease duration and age at seizure onset; Meng's z-test; Supplementary Fig. 5C).

Discussion

Together with the multisite ENIGMA-Epilepsy initiative,[34,36,52,87] we investigated patterns of atypical inter-hemispheric asymmetry of cortical thickness and cross-sectional regional atrophy in a large sample of TLE patients and healthy controls. In particular, we studied whether (i) the spatial distribution of atypical inter-hemispheric asymmetry differed from patterns of regional atrophy in TLE relative to controls; (ii) these patterns follow different topographic principles of cortical organization, particularly with respect to microstructural and functional gradients; and (iii) these effects showed a differential association to effects of epilepsy duration and age of onset. We found that atypical inter-hemispheric asymmetry analysis and regional atrophy mapping provide complementary insights into the pathology of TLE *in vivo*, with atypical asymmetry showing an ipsilateral limbic signature, while cross-sectional cortical thickness mapping indicated widespread and bilateral atrophy in TLE. Atypical asymmetry and atrophy patterns of the cortex were also differentially associated with microstructural and functional gradients representing core axes of cortical organization,[39–41,44,88] supporting a topographic divergence of these two characterizations of TLE-related pathology. Findings were consistent across different sites and participants, corroborating generalizability. While cortical atrophy was correlated with disease duration and age at seizure onset, atypical asymmetry did not show an association to these variables. Collectively, our study underscores complementarity of atypical asymmetry and atrophy

mapping for *in vivo* pathology mapping, which will be relevant for future imaging biomarker discovery and validation efforts.

In managing TLE patients, preoperative lateralization of temporal lobe pathology is key to define the surgical target and often relies on the qualitative visual assessment of inter-hemispheric asymmetry. Quantitative imaging analyses in clinical and research settings can be geared towards the identification of asymmetry, and several prior studies have systematically investigated between-hemisphere differences in grey matter morphological measures in TLE. Most of these studies have focused on the asymmetry of the hippocampus and adjacent mesiotemporal structures, suggesting marked limbic structural asymmetry in TLE.[19,21,37,89] Asymmetry analysis has several benefits, including the ability to use a given patient as their own baseline while controlling for corresponding measures in controls. However, the field lacks systematic analyses of asymmetry, particularly outside the mesiotemporal region. There have been no quantitative comparisons of atypical inter-hemispheric asymmetry with maps of cross-sectional regional atrophy mapping, in which measures in patients with TLE are compared to groups of healthy controls. When carried out in structures of the limbic system, atrophy mapping also reveals structural compromise in TLE compared to healthy controls, with variable degrees of asymmetry ranging from relatively ipsilateral to rather bilateral depending on the TLE subgroups.[10,15,19] The advent of automated morphometric analysis has resulted in a predominance of studies focusing on cross-sectional regional thickness comparisons, and relatively few large-scale analyses have assessed the topography of atypical cortical thickness asymmetry patterns in TLE.[31–35,38] Notably, although atypical asymmetry and atrophy are sometimes used interchangeably in the neuroimaging literature of TLE as *in vivo* indices of pathology, our findings pointed to differences in the topography of atypical cortical asymmetry and regional patterns of cross-sectional atrophy in TLE. Spatial correlation analysis confirmed this, failing to identify an association between these spatial patterns after accounting for spatial autocorrelations. Atypical asymmetry in TLE followed a more specific paralimbic topography with maximal effects in the mesiotemporal lobe, in line with the classical conceptualizations of TLE as a limbic network disorder.[1–3,90] On the other hand, in line with prior single site analyses[28–31] and recent ENIGMA-Epilepsy studies,[34,36,52] regional cortical atrophy mapping confirmed ipsilateral mesiotemporal atrophy in TLE, as well as widespread and bilateral effects outside paralimbic cortical areas. Findings were consistent in both left and right TLE patients. Thus, and despite both left and right TLE groups potentially showing different structural compromise,[21,34,62,91–94] findings overall suggest a similar divergence of atrophy and asymmetry patterns irrespective of seizure focus lateralization.

Our findings were further contextualized by quantifying the alignment of asymmetry and atrophy patterns along microstructural and functional gradients.[39–41] Cortical microstructural gradients place sensorimotor cortices with strong laminar differentiation and high myelin content at one end and paralimbic regions with subtle myelination, low laminar differentiation and increased synaptic densities at the other end.[41,72] Microstructural gradients, preserved across species,[41,72,95] follow canonical models of sensory–fugal cortical hierarchies[88] and capture inter-regional variations in heritability and plasticity.[96] While also starting at sensorimotor systems, the principal functional gradient radiates towards transmodal networks, such as the default mode and frontoparietal systems, and not the paralimbic cortices.[39] This divergence between microstructural and functional gradients may relate to less tethering of phylogenetically more recent association networks, such as the default mode network, from underlying signalling molecules[97] and may more closely reflect macroscale
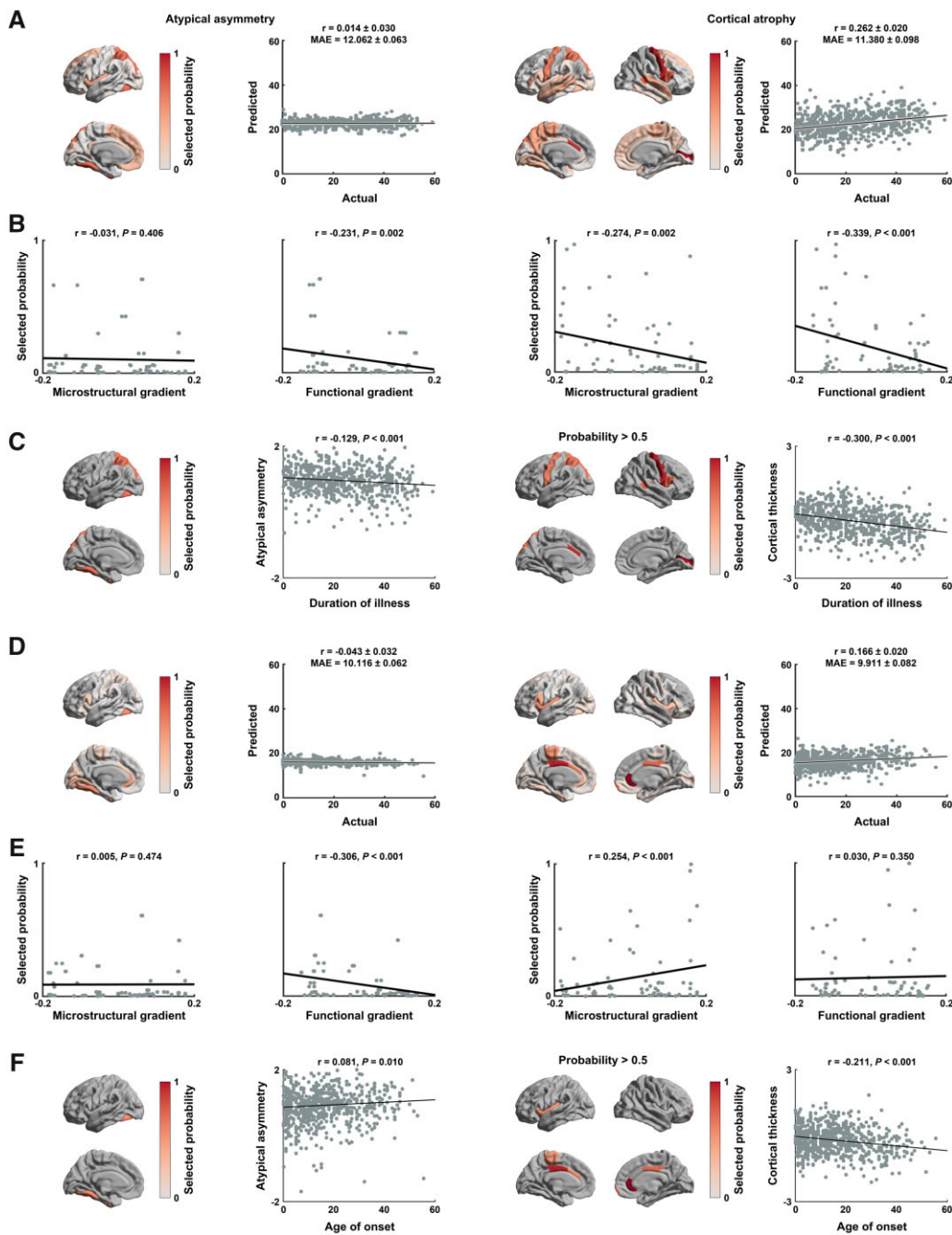
Figure 3 Associations between cortical features and clinical variables. (A) Probability of regions being selected across 5-fold nested cross-validation and 100 repetitions for predicting duration of epilepsy using atypical asymmetry index (*left*) and regional atrophy (*right*). Correlations between actual and predicted values of epilepsy duration are reported in the scatter plots. Black lines indicate the mean correlation and grey lines represent the 95% CI for 100 iterations with different training/test datasets. (B) Linear correlations between gradients and selected probability. (C) Spatial correlations between duration of epilepsy and atypical asymmetry index (*left*), as well as cortical atrophy (*right*) in highly probable (selected probability > 0.5) regions. (D–F) Identical analysis to A–C, but with respect to age at seizure onset. MAE = mean absolute error.

functional organization.[67] Spatial correlation analyses supported the dissociation of atypical cortical asymmetry and atrophy patterns with respect to microstructural gradients, where we observed increasing degrees of asymmetry towards the temporolimbic anchor of the microstructural gradient, while atrophy patterns increased towards primary sensorimotor and unimodal association areas. While confirming stronger effects towards sensorimotor anchors in the case of atrophy patterns, functional gradient associations were less conclusive about atypical asymmetry, indirectly underscoring the paralimbic pattern of the latter.

Furthermore, these findings may indicate that cortical morphological changes are better captured by microstructural than by functional hierarchies, a finding echoing prior associations between intracortical cellular-synaptic factors and measures of cortical thickness.[98–101] Both cortical thickness and microstructural gradients were derived from structural MRI and thickness and intracortical myelin are largely related to cortical cytoarchitecture,[45,102] which could indeed explain a strong correlation between atrophy and the microstructural gradient. It is, nevertheless, important to point out that cortical thickness and intracortical

microstructural measures were calculated using different approaches: (i) cortical thickness was measured as the distance between pial and white matter cortical interfaces from T_1-weighted data, tapping into overall cortical morphology; while (ii) the microstructural gradient was derived from depth-dependent intracortical intensity profiles based on the ratio of T_1- and T_2-weighted data from the HCP dataset (and from quantitative T_1 relaxometry data in the case of the local MICs dataset). Prior research has furthermore shown that cortical morphology as indexed by cortical thickness measures as well as internal cortical microstructure reflects likely complementary aspects of healthy and diseased brain organization. For example, age-related effects on cortical thinning and myelination do not occur in parallel, but rather in a different spatial distribution during typical development[45,102] as well as lifespan.[103–106] In TLE, it has been shown that changes in intracortical microstructure based on quantitative T_1 relaxometry occur above and beyond changes in MRI-based cortical thickness, suggesting that potentially different biological and pathological processes drive changes in morphology and microstructure in the condition.[107]

Big data initiatives such as ENIGMA-Epilepsy offer increased sensitivity to identify disease-related patterns of structural compromise. Extending from initial meta-analysis efforts,[34] it is furthermore possible to assess consistency of findings at the single site and individual patient levels. Here, we observed that the dissociation between atypical cortical asymmetry and atrophy remained consistent when we considered individual sites separately, and to some degree also at the level of individual participants. Using machine learning, we associated cortex-wide morphological data with clinical variables and showed inter-individual differences in cortical atrophy associated with disease duration and age at seizure onset. Associations were primarily driven by primary regions in sensorimotor cortex, together with temporal cortices and the precuneus. Unlike cortical thickness, atypical asymmetry patterns were not significantly associated with these clinical variables. These divergent clinical associations suggest that atypical inter-hemispheric asymmetry and regional cortical atrophy potentially reflect different TLE pathological processes, with asymmetry being more specifically related to an initial insult of the limbic circuitry. Alternatively, patterns of TLE-related atrophy in widespread and bilateral cortical territories had apparent progressive effects. The latter finding is consistent with prior cross-sectional, longitudinal and meta-analytic findings assessing disease progression effects in TLE.[29,32,91,108–111] This effect may relate to ongoing seizures, as supported by prior data showing associations to seizure frequency,[91,110,111] as well as from anti-epileptic drug treatment.[112,113] Moreover, drug-resistant patients are at increased risk for mood disorders and psychosocial challenges,[114] which may furthermore adversely impact brain health.

We found that measures of atypical asymmetry and atrophy provide complementary windows into structural compromise in TLE, a finding also supported by the differential relationships to cortical topographic gradients and diverging associations to clinical parameters. Our findings advance our understanding of large-scale pathology in TLE and may direct future discovery and validation of clinically useful neuroimaging biomarkers.

Acknowledgements

Funding

Competing interests

P.M.T. received grant support from Biogen, Inc., and consulting payments from Kairos Venture Capital, for work unrelated to the current manuscript. All other authors report no competing interests.

Supplementary material

Supplementary material is available at *Brain* online.

References

1. Falconer MA, Serafetinides EA, Corsellis JAN. Etiology and pathogenesis of temporal lobe epilepsy. *Arch Neurol*. 1964; 10(3):233–248.

2. Margerison JH, Corsellis JAN. Epilepsy and the temporal lobes. *Brain*. 1966;89(3):499–530.

3. Blanc F, Martinian L, Liagkouras I, Catarino C, Sisodiya SM, Thom M. Investigation of widespread neocortical pathology associated with hippocampal sclerosis in epilepsy: A postmortem study. *Epilepsia*. 2011;52(1):10–21.

4. Blümcke I, Thom M, Aronica E, et al. International consensus classification of hippocampal sclerosis in temporal lobe epilepsy: A Task Force report from the ILAE Commission on Diagnostic Methods. *Epilepsia*. 2013;54(7):1315–1329.

5. Thom M. Review: Hippocampal sclerosis in epilepsy: A neuropathology review. *Neuropathol Appl Neurobiol*. 2014;40(5):520–543.

6. Bartolomei F, Khalil M, Wendling F, et al. Entorhinal cortex involvement in human mesial temporal lobe epilepsy: An electrophysiologic and volumetric study. *Epilepsia*. 2005;46(5):677–687.

7. Ogren JA, Wilson CL, Bragin A, et al. Three-dimensional surface maps link local atrophy and fast ripples in human epileptic hippocampus. *Ann Neurol*. 2009;66(6):783–791.

8. Wiebe S, Blume WT, Girvin JP, Eliasziw M. A randomized, controlled trial of surgery for temporal-lobe epilepsy. *N Engl J Med*. 2001;345(5):311–318.

9. de Tisi J, Bell GS, Peacock JL, et al. The long-term outcome of adult epilepsy surgery, patterns of seizure remission, and relapse: A cohort study. *Lancet*. 2011;378(9800):1388–1395.

10. Bernhardt BC, Hong SJ, Bernasconi A, Bernasconi N. Magnetic resonance imaging pattern learning in temporal lobe epilepsy: Classification and prognostics. *Ann Neurol*. 2015;77(3):436–446.

11. Bernhardt BC, Hong S, Bernasconi A, Bernasconi N. Imaging structural and functional brain networks in temporal lobe epilepsy. *Front Hum Neurosci*. 2013;7:624.

12. Winston GP, Micallef C, Kendell BE, et al. The value of repeat neuroimaging for epilepsy at a tertiary referral centre: 16 years of experience. *Epilepsy Res*. 2013;105(3):349–355.

13. Larivière S, Bernasconi A, Bernasconi N, Bernhardt BC. Connectome biomarkers of drug-resistant epilepsy. *Epilepsia*. 2020;62(1):6–19.

14. Cascino GD, Jack CR, Parisi JE, et al. Magnetic resonance imaging-based volume studies in temporal lobe epilepsy: Pathological correlations. *Ann Neurol*. 1991;30(1):31–36.

15. Cendes F, Leproux F, Melanson D, et al. MRI of amygdala and hippocampus in temporal lobe epilepsy. *J Comput Assist Tomogr*. 1993;17(2):206–210.

16. van Paesschen W, Sisodiya S, Connelly A, et al. Quantitative hippocampal MRI and intractable temporal lobe epilepsy. *Neurology*. 1995;45(12):2233–2240.

17. Kuzniecky RI, Bilir E, Gilliam F, et al. Multimodality MRI in mesial temporal sclerosis: Relative sensitivity and specificity. *Neurology*. 1997;49(3):774–778.

18. Briellmann RS, Jackson GD, Kalnins R, Berkovic SF. Hemicranial volume deficits in patients with temporal lobe epilepsy with and without hippocampal sclerosis. *Epilepsia*. 1998;39(11):1174–1181.

19. Bernasconi N, Bernasconi A, Caramanos Z, Antel SB, Andermann F, Arnold DL. Mesial temporal damage in temporal lobe epilepsy: A volumetric MRI study of the hippocampus, amygdala and parahippocampal region. *Brain*. 2003;126(Pt 2):462–469.

20. Bonilha L, Rorden C, Castellano G, et al. Voxel-based morphometry reveals gray matter network atrophy in refractory medial temporal lobe epilepsy. *Arch Neurol*. 2004;61(9):1379–1384.

21. Bonilha L, Rorden C, Halford JJ, et al. Asymmetrical extra-hippocampal grey matter loss related to hippocampal atrophy in patients with medial temporal lobe epilepsy. *J Neurol Neurosurg Psychiatry*. 2007;78(3):286–294.

22. Seidenberg M, Kelly KG, Parrish J, et al. Ipsilateral and contralateral MRI volumetric abnormalities in chronic unilateral temporal lobe epilepsy and their clinical correlates. *Epilepsia*. 2005;46(3):420–430.

23. Pulsipher DT, Seidenberg M, Morton JJ, Geary E, Parrish J, Hermann B. MRI volume loss of subcortical structures in unilateral temporal lobe epilepsy. *Epilepsy Behav*. 2007;11(3):442–449.

24. Keller SS, Roberts N. Voxel-based morphometry of temporal lobe epilepsy: An introduction and review of the literature. *Epilepsia*. 2008;49(5):741–757.

25. Bonilha L, Halford JJ, Riederer F, Baumgartner C. Network atrophy in temporal lobe epilepsy: A voxel-based morphometry study. *Neurology*. 2009;72(23):2052–2052.

26. Bonilha L, Rorden C, Castellano G, Cendes F, Li LM. Voxel-based morphometry of the thalamus in patients with refractory medial temporal lobe epilepsy. *Neuroimage*. 2005;25(3):1016–1021.

27. Bonilha L, Elm JJ, Edwards JC, et al. How common is brain atrophy in patients with medial temporal lobe epilepsy? *Epilepsia*. 2010;51(9):1774–1779.

28. Lin JJ, Salamon N, Lee AD, et al. Reduced neocortical thickness and complexity mapped in mesial temporal lobe epilepsy with hippocampal sclerosis. *Cereb Cortex*. 2007;17(9):2007–2018.

29. Bernhardt BC, Bernasconi N, Concha L, Bernasconi A. Cortical thickness analysis in temporal lobe epilepsy: Reproducibility and relation to outcome. *Neurology*. 2010;74(22):1776–1784.

30. Bernhardt BC, Worsley KJ, Besson P, et al. Mapping limbic network organization in temporal lobe epilepsy using morphometric correlations: Insights on the relation between mesiotemporal connectivity and cortical atrophy. *Neuroimage*. 2008;42(2):515–524.

31. McDonald CR, Hagler DJ, Ahmadi ME, et al. Regional neocortical thinning in mesial temporal lobe epilepsy. *Epilepsia*. 2008;49(5):794–803.

32. Galovic M, Van Dooren VQH, Postma TS, et al. Progressive cortical thinning in patients with focal epilepsy. *JAMA Neurol*. 2019;76(10):1230–1239.

33. Bernhardt BC, Rozen DA, Worsley KJ, Evans AC, Bernasconi N, Bernasconi A. Thalamo-cortical network pathology in idiopathic generalized epilepsy: Insights from MRI-based morphometric correlation analysis. *Neuroimage*. 2009;46(2):373–381.

34. Whelan CD, Altmann A, Botía JA, et al. Structural brain abnormalities in the common epilepsies assessed in a worldwide ENIGMA study. *Brain*. 2018;141(2):391–408.

35. Weng Y, Larivière S, Caciagli L, et al. Macroscale and microcircuit dissociation of focal and generalized human epilepsies. *Commun Biol*. 2020;3(1):1–11.

36. Sisodiya SM, Whelan CD, Hatton SN, et al.; ENIGMA Consortium Epilepsy Working Group. The ENIGMA-Epilepsy working group: Mapping disease from large data sets. *Hum Brain Mapp*. 2020;1–16.

37. Bonilha L, Kobayashi E, Rorden C, Cendes F, Li LM. Medial temporal lobe atrophy in patients with refractory temporal lobe epilepsy. *J Neurol Neurosurg Psychiatry*. 2003;74(12):1627–1630.

38. Alhusaini S, Doherty CP, Palaniyappan L, et al. Asymmetric cortical surface area and morphology changes in mesial temporal lobe epilepsy with hippocampal sclerosis. *Epilepsia*. 2012;53(6):995–1003.

39. Margulies DS, Ghosh SS, Goulas A, et al. Situating the default-mode network along a principal gradient of macroscale cortical organization. *Proc Natl Acad Sci USA*. 2016;113(44):12574–12579.

40. Huntenburg JM, Bazin PL, Margulies DS. Large-scale gradients in human cortical organization. *Trends Cogn Sci.* 2018;22(1): 21–31.

41. Paquola C, Vos De Wael R, Wagstyl K, et al. Microstructural and functional gradients are increasingly dissociated in trans-modal cortices. *PLoS Biol.* 2019;17(5):e3000284.

42. Deco G, Ponce-Alvarez A, Mantini D, Romani GL, Hagmann P, Corbetta M. Resting-state functional connectivity emerges from structurally and dynamically shaped slow linear fluctuations. *J Neurosci.* 2013;33(27):11239–11252.

43. Wang P, Knösche TR. A realistic neural mass model of the cortex with laminar-specific connections and synaptic plasticity—Evaluation with auditory habituation. *PLoS One.* 2013; 8(10):e77876.

44. Burt JB, Demirtaş M, Eckner WJ, et al. Hierarchy of transcriptomic specialization across human cortex captured by structural neuroimaging topography. *Nat Neurosci.* 2018;21(9): 1251–1259.

45. Paquola C, Bethlehem RA, Seidlitz J, et al.; NSPN Consortium. Shifts in myeloarchitecture characterise adolescent development of cortical gradients. *eLife.* 2019;8:e50482.

46. Wang XJ. Macroscopic gradients of synaptic excitation and inhibition in the neocortex. *Nat Rev Neurosci.* 2020;21(3):169–178.

47. Flechsig Of Leipsic P. Developmental (myelogenetic) localisation of the cerebral cortex in the human subject. *Lancet.* 1901; 158(4077):1027–1030.

48. Barbas H, García-Cabezas M. Motor cortex layer 4: Less is more. *Trends Neurosci.* 2015;38(5):259–261.

49. Palomero-Gallagher N, Zilles K. Cortical layers: Cyto-, myelo-, receptor- and synaptic architecture in human cortical areas. *Neuroimage.* 2019;197:716–741.

50. Drenthen GS, Backes WH, Aldenkamp AP, Vermeulen RJ, Klinkenberg S, Jansen JFA. On the merits of non-invasive myelin imaging in epilepsy, a literature review. *J Neurosci Methods.* 2020;338:108687.

51. Vos de Wael R, Benkarim O, Paquola C, et al. BrainSpace: A toolbox for the analysis of macroscale gradients in neuroimaging and connectomics data sets. *Commun Biol.* 2020;3(1):103.

52. Larivière S, Rodríguez-Cruces R, Royer J, et al. Network-based atrophy modelling in the common epilepsies: A worldwide ENIGMA study. *Sci Adv.* 2020;6:eabc6457.

53. Berg AT, Berkovic SF, Brodie MJ, et al. Revised terminology and concepts for organization of seizures and epilepsies: Report of the ILAE Commission on Classification and Terminology, 2005–2009. *Epilepsia.* 2010;51(4):676–685.

54. Van Essen DC, Smith SM, Barch DM, Behrens TEJ, Yacoub E, Ugurbil K, WU-Minn HCP Consortium. The WU-Minn Human Connectome Project: An overview. *Neuroimage.* 2013;80:62–79.

55. Fischl B. FreeSurfer. *Neuroimage.* 2012;62(2):774–781.

56. Jenkinson M, Beckmann CF, Behrens TEJ, Woolrich MW, Smith SM. FSL. *Neuroimage.* 2012;62(2):782–790.

57. Glasser MF, Sotiropoulos SN, Wilson JA, et al.; WU-Minn HCP Consortium. The minimal preprocessing pipelines for the Human Connectome Project. *Neuroimage.* 2013;80:105–124.

58. Cox RW. AFNI: Software for analysis and visualization of functional magnetic resonance neuroimages. *Comput Biomed Res.* 1996;29(3):162–173.

59. Avants BB, Tustison NJ, Song G, Cook PA, Klein A, Gee JC. A reproducible evaluation of ANTs similarity metric performance in brain image registration. *Neuroimage.* 2011;54(3):2033–2044.

60. Kong XZ, Mathias SR, Guadalupe T, et al.; ENIGMA Laterality Working Group. Mapping cortical brain asymmetry in 17,141 healthy individuals worldwide via the ENIGMA consortium. *Proc Natl Acad Sci USA.* 2018;115(22):E5154–E5163.

61. Sarica A, Vasta R, Novellino F, Vaccaro MG, Cerasa A, Quattrone A. MRI asymmetry index of hippocampal subfields increases through the continuum from the mild cognitive impairment to the Alzheimer's disease. *Front Neurosci.* 2018;12: 576.

62. Liu M, Bernhardt BC, Bernasconi A, Bernasconi N. Gray matter structural compromise is equally distributed in left and right temporal lobe epilepsy. *Hum Brain Mapp.* 2016;37(2):515–524.

63. Johnson WE, Li C, Rabinovic A. Adjusting batch effects in microarray expression data using empirical Bayes methods. *Biostatistics.* 2007;8(1):118–127.

64. Fortin JP, Cullen N, Sheline YI, et al. Harmonization of cortical thickness measurements across scanners and sites. *Neuroimage.* 2018;167:104–120.

65. Worsley KJ, Taylor JE, Carbonell F, et al. SurfStat: A Matlab toolbox for the statistical analysis of univariate and multivariate surface and volumetric data using linear mixed effects models and random field theory. *Neuroimage.* 2009;47(Suppl):S102.

66. Benjamini Y, Hochberg Y. Controlling the false discovery rate: A practical and powerful approach to multiple testing. *J R Stat Soc.* 1995;57(1):289–300.

67. Yeo BTT, Krienen FM, Sepulcre J, et al. The organization of the human cerebral cortex estimated by intrinsic functional connectivity. *J Neurophysiol.* 2011;106(3):1125–1165.

68. Hong SJ, Xu T, Nikolaidis A, et al. Toward a connectivity gradient-based framework for reproducible biomarker discovery. *Neuroimage.* 2020;223:117322.

69. Hong S-J, Vos De Wael R, Bethlehem RAI, et al. Atypical functional connectome hierarchy in autism. *Nat Commun.* 2019; 10(1):1022-

70. Valk SL, Xu T, Margulies DS, et al. Shaping brain structure: Genetic and phylogenetic axes of macroscale organization of cortical thickness. *Sci Adv.* 2020;6(39):1–15.

71. Müller EJ, Munn B, Hearne LJ, et al. Core and matrix thalamic sub-populations relate to spatio-temporal cortical connectivity gradients. *Neuroimage.* 2020;222:117224.

72. Huntenburg JM, Bazin PL, Goulas A, Tardif CL, Villringer A, Margulies DS. A systematic relationship between functional connectivity and intracortical myelin in the human cerebral cortex. *Cereb Cortex.* 2017;27(2):981–997.

73. Park B, Vos de Wael R, Paquola C, et al. Signal diffusion along connectome gradients and inter-hub routing differentially contribute to dynamic human brain function. *Neuroimage.* 2021;224:117429.

74. Larivière S, Vos de Wael R, Hong S-J, et al. Multiscale structure–function gradients in the neonatal connectome. *Cereb Cortex.* 2020;30(1):47–58.

75. Coifman RR, Lafon S. Diffusion maps. *Appl Comput Harmon Anal.* 2006;21(1):5–30.

76. Tenenbaum JB, V de S, Langford JC. A global geometric framework for nonlinear dimensionality reduction. *Science.* 2000; 290(5500):2319–2323.

77. von Luxburg U. A tutorial on spectral clustering. *Stat Comput.* 2007;17(4):395–416.

78. Park B, Park H, Morys F, et al. Inter-individual body mass variations relate to fractionated functional brain hierarchies. *Commun Biol.* 2021;4(1):1–12.

79. Alexander-Bloch AF, Shou H, Liu S, et al. On testing for spatial correspondence between maps of human brain structure and function. *Neuroimage.* 2018;178:540–551.

80. Larivière S, Paquola C, Park B, et al. The ENIGMA toolbox: Multiscale neural contextualization of multisite neuroimaging data sets. *Nat Methods.* 2021;18(7):698–700.

81. Varma S, Simon R. Bias in error estimation when using cross-validation for model selection. *BMC Bioinformatics.* 2006;7:91.

82. Cawley GC, Talbot NLC. On over-fitting in model selection and subsequent selection bias in performance evaluation. *J Mach Learn Res*. 2010;11:2079–2107.

83. Parvandeh S, Yeh HW, Paulus MP, McKinney BA. Consensus features nested cross-validation. *Bioinformatics*. 2020;36(10):3093–3098.

84. Tibshirani R. Regression shrinkage and selection via the LASSO. *J R Stat Soc Ser B*. 1996;58(1):267–288.

85. Meng XL, Rosenthal R, Rubin DB. Comparing correlated correlation coefficients. *Psychol Bull*. 1992;111(1):172–175.

86. Desikan RS, Ségonne F, Fischl B, et al. An automated labeling system for subdividing the human cerebral cortex on MRI scans into gyral based regions of interest. *Neuroimage*. 2006;31(3):968–980.

87. Thompson PM, Jahanshad N, Ching CRK, et al.; ENIGMA Consortium. ENIGMA and global neuroscience: A decade of large-scale studies of the brain in health and disease across more than 40 countries. *Transl Psychiatry*. 2020;10(1):100.

88. Mesulam MM. From sensation to cognition. *Brain*. 1998;121(6):1013–1052.

89. Shah P, Bassett DS, Wisse LEM, et al. Structural and functional asymmetry of medial temporal subregions in unilateral temporal lobe epilepsy: A 7T MRI study. *Hum Brain Mapp*. 2019;40(8):2390–2398.

90. Tavakol S, Royer J, Lowe AJ, et al. Neuroimaging and connectomics of drug-resistant epilepsy at multiple scales: From focal lesions to macroscale networks. *Epilepsia*. 2019;60(4):593–604.

91. Coan AC, Appenzeller S, Bonilha L, Li LM, Cendes F. Seizure frequency and lateralization affect progression of atrophy in temporal lobe epilepsy. *Neurology*. 2009;73(11):834–842.

92. Santana MTCG, Jackowski AP, da Silva HH, et al. Auras and clinical features in temporal lobe epilepsy: A new approach on the basis of voxel-based morphometry. *Epilepsy Res*. 2010;89(2-3):327–338.

93. Kemmotsu N, Girard HM, Bernhardt BC, et al. MRI analysis in temporal lobe epilepsy: Cortical thinning and white matter disruptions are related to side of seizure onset. *Epilepsia*. 2011;52(12):2257–2266.

94. Dabbs K, Becker T, Jones J, Rutecki P, Seidenberg M, Hermann B. Brain structure and aging in chronic temporal lobe epilepsy. *Epilepsia*. 2012;53(6):1033–1043.

95. Fulcher BD, Murray JD, Zerbi V, Wang XJ. Multimodal gradients across mouse cortex. *Proc Natl Acad Sci USA*. 2019;116(10):4689–4695.

96. Vainik U, Paquola C, Wang X et al. Heritability of cortical morphology reflects a sensory–fugal plasticity gradient. *bioRxiv*. [Preprint] https://doi.org/10.1101/2020.11.03.366419

97. Buckner RL, Krienen FM. The evolution of distributed association networks in the human brain. *Trends Cogn Sci*. 2013;17(12):648–665.

98. Barbas H, Pandya DN. Architecture and intrinsic connections of the prefrontal cortex in the rhesus monkey. *J Comp Neurol*. 1989;286(3):353–375.

99. Herculano-Houzel S, Watson C, Paxinos G. Distribution of neurons in functional areas of the mouse cerebral cortex reveals quantitatively different cortical zones. *Front Neuroanat*. 2013;7:35.

100. Tomassy GS, Berger DR, Chen H-H, et al. Distinct profiles of myelin distribution along single axons of pyramidal neurons in the neocortex. *Science*. 2014;344(6181):319–324.

101. Suminaite D, Lyons DA, Livesey MR. Myelinated axon physiology and regulation of neural circuit function. *Glia*. 2019;67(11):2050–2062.

102. Whitaker KJ, Vértes PE, Romero-Garciaa R, et al.; NSPN Consortium. Adolescence is associated with genomically patterned consolidation of the hubs of the human brain connectome. *Proc Natl Acad Sci USA*. 2016;113(32):9105–9110.

103. Fjell AM, Grydeland H, Krogsrud SK, et al. Development and aging of cortical thickness correspond to genetic organization patterns. *Proc Natl Acad Sci USA*. 2015;112(50):15462–15467.

104. Tamnes CK, Herting MM, Goddings AL, et al. Development of the cerebral cortex across adolescence: A multisample study of inter-related longitudinal changes in cortical volume, surface area, and thickness. *J Neurosci*. 2017;37(12):3402–3412.

105. Tamnes CK, Roalf DR, Goddings AL, Lebel C. Diffusion MRI of white matter microstructure development in childhood and adolescence: Methods, challenges and progress. *Dev Cogn Neurosci*. 2018;33:161–175.

106. Tamnes CK, Østby Y, Fjell AM, Westlye LT, Due-Tønnessen P, Walhovd KB. Brain maturation in adolescence and young adulthood: Regional age-related changes in cortical thickness and white matter volume and microstructure. *Cereb Cortex*. 2010;20(3):534–548.

107. Bernhardt BC, Fadaie F, Vos de Wael R, et al. Preferential susceptibility of limbic cortices to microstructural damage in temporal lobe epilepsy: A quantitative T_1 mapping study. *Neuroimage*. 2018;182:294–303.

108. Bernhardt BC, Worsley KJ, Kim H, Evans AC, Bernasconi A, Bernasconi N. Longitudinal and cross-sectional analysis of atrophy in pharmacoresistant temporal lobe epilepsy. *Neurology*. 2009;72(20):1747–1754.

109. Bernhardt BC, Kim H, Bernasconi N. Patterns of subregional mesiotemporal disease progression in temporal lobe epilepsy. *Neurology*. 2013;81(21):1840–1847.

110. Caciagli L, Bernasconi A, Wiebe S, Koepp MJ, Bernasconi N, Bernhardt BC. A meta-analysis on progressive atrophy in intractable temporal lobe epilepsy: Time is brain? *Neurology*. 2017;89(5):506–516.

111. Bonilha L, Rorden C, Appenzeller S, Carolina Coan A, Cendes F, Min Li L. Gray matter atrophy associated with duration of temporal lobe epilepsy. *Neuroimage*. 2006;32(3):1070–1079.

112. Caciagli L, Xiao F, Wandschneider B, Koepp MJ. Imaging biomarkers of anti-epileptic drug action: Insights from magnetic resonance imaging. *Curr Pharm Des*. 2017;23(37):5727–5739.

113. Pardoe HR, Berg AT, Jackson GD. Sodium valproate use is associated with reduced parietal lobe thickness and brain volume. *Neurology*. 2013;80(20):1895–1900.

114. Lin JJ, Mula M, Hermann BP. Uncovering the neurobehavioural comorbidities of epilepsy over the lifespan. *Lancet*. 2012;380(9848):1180–1192.